Importance of Intersystem Crossing in the S(^{3}P, ^{1}D) + H_2 → SH + H Reaction†

Biswajit Maiti and George C. Schatz*

Department of Chemistry, Northwestern University, Evanston, Illinois 60208-3113

György Lendvay

Institute of Chemistry, Hungarian Academy of Sciences, P.O. Box 17, H-1525 Budapest, Hungary

Received: February 26, 2004; In Final Form: March 23, 2004

A "mixed" representation approach in conjunction with a trajectory surface-hopping method is used to study intersystem crossing effects in the S + H_2 reaction. These calculations are based on high-quality potential surfaces that we have determined for the two lowest triplet states of SH_2 and globally determined spin−orbit coupling matrix elements that are obtained from CASSCF calculations. A previously determined surface for the lowest singlet state (Ho, T.-S.; Hollebeek, T.; Rabitz, H.; Chao, S. D.; Skodje, R. T.; Zyubin, A. S.; Mebel, A. M. *J. Chem. Phys.* **2002**, *116*, 4124) is also used. We find that in contrast to the O(^{3}P) + H_2 reaction, which we studied previously at the same level, there is significant intersystem crossing in the S(^{3}P) + H_2 reaction. In particular, for the reaction starting from triplet S + H_2 close to the threshold, the dominant mechanism involves intersystem crossing to the singlet state prior to encountering the triplet barrier, and as a result, the thermal rate constant at low temperatures is controlled by intersystem crossing. This behavior occurs in part because the spin−orbit coupling is about 3 times larger in S than in O, but another important factor is the location of the singlet/triplet crossing, which occurs on the reagent side of the triplet barrier in S + H_2 and on the product side in O + H_2. We also find that trajectories that undergo a triplet-to-singlet transition have higher product rotational excitation than those that remain on the triplet surfaces. For the S(^{1}D) + H_2 reaction, we find significant electronic quenching due to intersystem crossing, leading to a factor of 2 or more reduction in the reactive cross section, and a much flatter dependence of the cross section on collision energy for energies above 2.5 kcal/mol. This result agrees with recent molecular beam measurements.

I. Introduction

Intersystem crossing (ISC) effects due to spin−orbit coupling are a subject of growing interest in fields ranging from chemical physics to chemical biology. Many enzymatic processes involve spin-forbidden steps; in addition, spin-forbidden dynamics plays a role in many gas-phase processes, including the quenching of excited states and reactions of high-spin ground-state radicals. In addition, there are many reactions that can take place via both spin-allowed and spin-forbidden pathways, in which case intersystem crossing influences the branching between products and details of the product energy partitioning. Recently, our group has started investigating very simple reactions for which intersystem crossing effects might play a role and for which high-level calculations (coupled potential energy surfaces and reaction dynamics) are possible. In our first studies, we examined the O(^{3}P)+H_2 reaction,[1,2] which is an important prototype for oxidation reactions to determine if the deep singlet H_2O well might be important in what is normally considered to be a purely triplet reaction. This is a nearly thermoneutral reaction with about a 13 kcal/mol barrier on the triplet surfaces. We found that the singlet state crosses the two lowest triplets mostly on the product side of the barrier, so although some collisions do sample the singlet surface, spin−orbit coupling has only a moderate effect on the dynamics of the system,[2] leading to about a 20% increase in reactive cross sections at energies that are 10 kcal/mol or more above the reactive threshold (no effect at all at energies close to threshold) and a corresponding enhancement in product rotational excitation. This effect is sufficiently subtle that it was not manifested in a recent crossed molecular beam experiment.[3]

The role of intersystem crossing in the S(^{3}P) + H_2 → SH +H reaction has long been a source of uncertainty. This is an endothermic reaction (by 19.8 kcal/mol) with a small exit channel barrier (2 kcal/mol relative to the product asymptote), so reaction can occur adiabatically on the two lowest triplet surfaces with an activation energy that is similar to the endothermicity. As with O + H_2, the lowest singlet state (correlating to S(^{1}D)) crosses the triplet to form a strongly bound H_2S intermediate and correlates to the same products, SH + H, as the triplet. In earlier studies of this reaction,[4] it was found that the singlet and triplet minimum-energy crossing is located before the triplet barrier and below the product asymptote in energy, thereby opening up the possibility that intersystem crossing would allow reaction to occur without surmounting the triplet barrier. Moreover, the spin−orbit constant of sulfur is roughly 3 times larger than that of O, therefore opening up the possibility that intersystem crossing will be both efficient and important. However, spin−orbit coupling dynamics studies were not considered in earlier work on S + H_2.

Past studies of S + H_2 as well as the thermal decomposition of H_2S provide hints but also confusion concerning the importance of intersystem crossing. For example, Woiki and Roth as well as Olschewski et al. observed the spin-forbidden decomposition of H_2S to give S(^{3}P) + H_2,[5,6] but studies by

† Part of the "Gert D. Billing Memorial Issue".

* Corresponding author. E-mail: schatz@chem.northwestern.edu.

10.1021/jp049143o CCC: $27.50
Published on Web 05/05/2004

Shiina et al. of the $S + H_2$[4,7] kinetics suggested that the Arrhenius preexponential factor is too large for a spin-forbidden reaction mechanism. Instead, the measured rate constant is similar to that for a spin-allowed H-atom abstraction reaction. Very recently, using kinetic modeling in conjunction with a continuous-flow, jet-mixed reactor, Binoist et al.[8] showed that the abstraction reaction is an important part of the dominant mechanism of the pyrolysis of H_2S. Spin-forbidden recombination of $S(^3P)$ with H_2 to give H_2S should also be possible, although Shiina at al.[7] were unable to observe pressure dependence in the $S + H_2$ rate constant for pressures up to 4 atm. They used a statistical theory result to estimate that pressures >120 atm would be needed at 900 K to make insertion significant, suggesting that the spin-forbidden insertion mechanism is relatively inefficient compared to the possibly spin-allowed abstraction.

In this paper, we have undertaken a detailed theoretical study of the $S(^3P, ^1D) + H_2$ reaction through the determination of global potential energy surfaces and spin−orbit couplings and using a trajectory surface-hopping method to describe the nonadiabatic dynamics. Our results show that there is significant intersystem crossing from the triplet to the singlet state during the course of the $S(^3P) + H_2$ reaction, providing an energetically more favorable reaction path that avoids the triplet barrier. This explains why the activation energy for the $S(^3P) + H_2$ reaction is about the same as the endothermicity of the reaction, as previously observed by Tsuchiya et al.[9] In addition, we find that intersystem crossing plays an important role in $S(^1D) + H_2$, and this explains the less-than-perfect agreement between theory and experiment noted in a recent study based on singlet-only dynamics.[10]

Our calculations are based on a theory of intersystem crossing that was developed in our earlier publication.[2] In this method, one uses global nonrelativistic potential energy surfaces corresponding to the interacting spin states together with spin−orbit coupling elements from CASSCF calculations to define the coupled electronic states. In the $S + H_2$ reaction, a full treatment would require 15 states (i.e., 9 triplets from the $^3P_2$, $^3P_1$, and $^3P_0$ levels of S and 6 singlets from $^1D_2$ and $^1S_0$), but the basis set can be truncated, following a procedure proposed by Hoffmann and Schatz.[1] In the truncated basis, the number of Born−Oppenheimer surfaces that are actively coupled in the intersystem crossing calculation is just four. Moreover, two of the four electronic basis functions are components of the same spin multiplet; therefore, we need only three Born−Oppenheimer surfaces.

The dynamics calculations use a quasiclassical trajectory surface-hopping (TSH) method based on a "mixed" representation, as recently described.[2] This representation turns into the adiabatic representation for geometries corresponding to the reactants and products, wherein the spin−orbit fine-structure states are properly defined, and it evolves to a diabatic representation when the singlet and triplet states cross at geometries where the three atoms are close together. As a result, we are using the adiabatic representation when the adiabats are weakly coupled and the diabatic representation when the diabats are weakly coupled, which is ideal for the success of the TSH method.

In the $S(^3P, ^1D) + H_2$ reaction, the most important low-energy singlet/triplet crossings are between the lowest component of $S(^1D)$, which is of $^1A'$ symmetry for bent SHH geometries, and the two lowest components of $S(^3P)$, which have $^3A''$ and $^3A'$ symmetry for nonlinear SHH. Figure 1 depicts a schematic

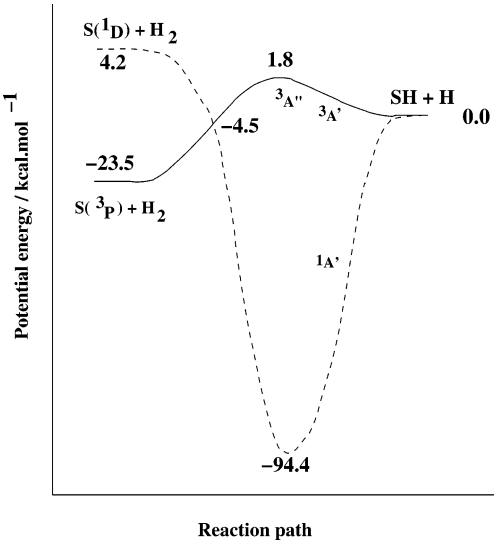

Figure 1. Schematic of singlet ($^1A'$) and triplet ($^3A'$ and $^3A''$) potential energy surfaces associated with the $S(^3P, ^1D) + H_2$ reaction. The curves approximately represent the potential along the minimum-energy path of the triplet reaction.

energy diagram along the reaction path for states $^3A'$, $^3A''$, and $^1A'$ based on ab initio calculations that are described below. Although the triplet-state reaction is endoergic by about 23.5 kcal/mol and has a 25.3 kcal/mol barrier for abstraction, the singlet-state surface is strongly attractive and involves an insertion reaction mechanism and the formation of a short-lived hydrogen sulfide (H_2S) intermediate complex in the singlet well (depth of about −94.4 kcal/mol). In the reagent region, $S(^1D) + H_2$ is about 27.7 kcal/mol above $S(^3P) + H_2$, and in the products region, the singlet and triplet states are degenerate and correlate to the same $SH(^2\Pi) + H$ product. Note that all energies in the Figure are relative to the product asymptote, SH + H. Earlier studies[4] found that the singlet−triplet crossing occurs before the triplet barrier, with a crossing energy that is below the product asymptote (at an energy of −4.5 kcal/mol). As a result, less energy is needed to cross into the singlet well than to surmount the barrier, providing a spin-forbidden pathway for reaction that is likely to be most important close to the reactive threshold. This is the most intriguing difference with respect to the $O(^3P) + H_2$ reaction because the singlet−triplet crossing for that reaction occurs on the product side of the triplet barrier and ISC has only a subtle effect[2] on the reaction dynamics. Shiina et al.[4] demonstrated that the lowest-energy singlet−triplet crossing occurs for the C_{2v} approach of the S atom to the hydrogen molecules, but the reaction path on the triplet surfaces corresponds to linear S−H−H geometry. This means that a reaction that takes place by ISC can involve a highly nonlinear approach of S to H_2, whereas the triplet-only dynamics is expected to involve nearly linear geometries. It is therefore of interest to determine whether this influences product translational or rotational distributions in an important way.

II. Computational Details

A. Potential Energy Surfaces and Spin−Orbit Matrix Elements. The singlet surface that we used in our calculation was from Ho et al.[10] This surface was based on multireference configuration interaction calculations with an augmented quadruple-ζ basis set. The surface was modified by adding 0.13626832898581 au globally to make the product SH + H asymptote the zero of energy and also to make the singlet and

TABLE 1: Parameters for the Switching Function f_{SW} Used to Define the Triplet Surfaces

parameters	values
$(r^0_{SH}, r^0_{HH})/a_0$	(3.0, 3.7)
$(\gamma_{SH}, \gamma_{HH})$	(1.0, 0.9)
α_0/deg	80.0
γ_α	1.0

triplet SH + H asymptotes degenerate. The two triplet surfaces were calculated at a lower level of theory, namely, QCISD(T) using Dunning's aug-cc-pVTZ basis set. Ab initio points were generated in internal coordinates on an equally spaced rectangular grid such that r_{SH} ranges from 1.2 to 2.6 Å, r_{HH} ranges from 0.7 to 2.3 Å with a 0.1-Å grid spacing and with the S−H−H angle varying from 80 to 180° in 10° steps. Global analytical triplet surfaces were generated using a 3D-spline interpolation method based on this grid. However, extrapolation based on spline interpolation gave spurious results near the asymptotes, which is outside of the range covered by the ab initio data. To fix this, the asymptotic behavior was described using an LEPS function based on parameters obtained by fitting Morse functions to the diatomic ab initio points (and taking the Sato parameters to be zero). The Morse parameters (in atomic units) are $D_e(H_2) = 0.17301$, $r_e(H_2) = 1.4088$, $\beta(H_2) = 1.0340$, $D_e(SH) = 0.13554$, $r_e(SH) = 2.5424$, and $\beta(SH) = 1.0183$. To generate global triplet potential energy surfaces, we switch from the spline-fitted ab initio points in the interaction region to the LEPS function near the asymptotes. The switching is done smoothly using a function defined as the product of three functions:

$$f(x) = \frac{1.0 - \tanh(\gamma(x - x_0))}{2.0} \text{ for coordinates } r_{SH} \text{ and } r_{HH}$$

and

$$f(x) = \frac{1.0 + \tanh(\gamma(x - x_0))}{2.0}$$

for angle α (the H−H−S internal angle)

where x represents coordinates r_{SH}, r_{HH}, and α, in general. The parameters used in the present calculations are listed in Table 1. The switching is done following the equation

$$v_{\text{triplet}} = f_{SW} \times v_{\text{ab initio}} + (1.0 - f_{SW}) \times v_{\text{LEPS}}$$

where f_{SW} is the product of switching functions.

Figure 2 presents contour plots of the singlet and the ground triplet potential energy surfaces in Jacobi coordinates (R, r) for a fixed angle $\theta = 30°$. Here r is the H−H distance, R is the distance of S from the center of mass of H_2, and θ is the angle between vectors R and r. The singlet−triplet crossing seam is also indicated. This Figure clearly shows that in contrast to O + H_2 → OH + H, S + H_2 → SH + H is a late barrier reaction. More interestingly, the singlet−triplet crossing is before the triplet barrier location and below the product asymptote. In Figure 3, we have plotted contours of the same potential energy surfaces but using the Jacobi coordinates (R, θ) for a fixed $r = 1.4a_0$ at its equilibrium value. This Figure indicates how the potential changes when the S atom approaches H_2 from different directions. It is seen that the seam location is almost independent of the angle θ beyond $\theta = 30°$, implying that the seam is accessible over a wide range of angles away from the linear S−H−H structure for energies that are about 5 kcal/mol below the product asymptote.

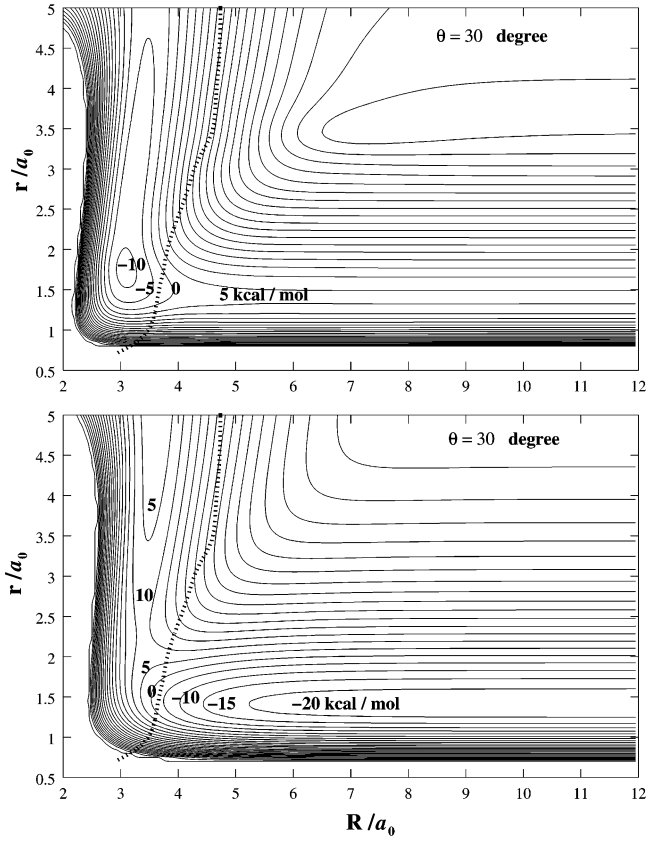

Figure 2. Contours of the $^1A'$ and $^3A''$ potential surfaces in Jacobi coordinates (R, r) for a fixed angle of $\theta = 30°$. The thick dotted line shows the seam of intersection between the two surfaces.

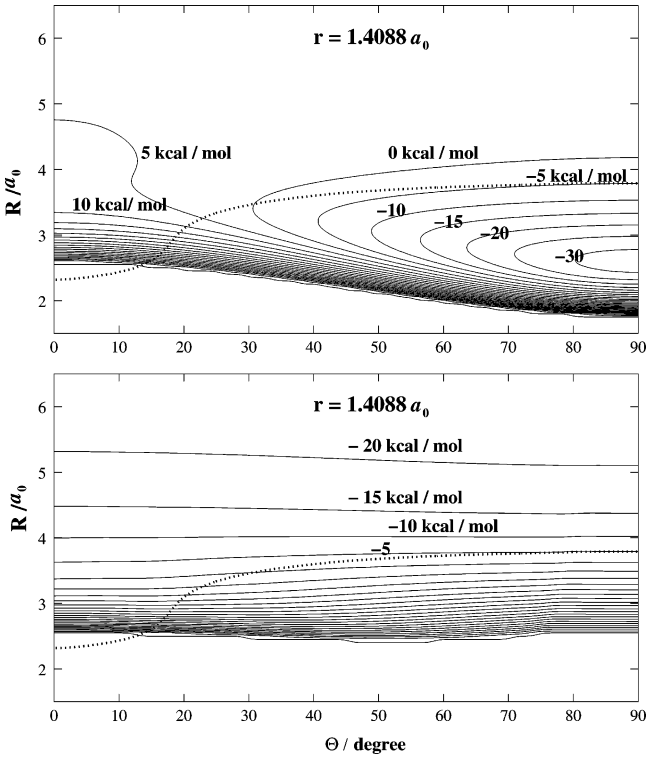

Figure 3. Contours of the $^1A'$ and $^3A''$ potential surfaces in Jacobi coordinates (R, θ) for fixed $r = 1.4a_0$. The thick dotted lines show the intersection seam.

There are 15 initial states (described above) for the S + H_2 reaction that one needs to consider to describe the reaction dynamics. These states are coupled in many different ways, but

here we are interested in intersystem crossing so we truncate the electronic basis to those states most directly coupled by spin−orbit interaction, namely, the two lowest triplets (i.e., two of the three triplets that correlate to the ground reagent state, leaving out the third one that correlates to an excited product state) and the lowest singlet state (which is the only state that crosses the lower two triplet states). Also, we have adapted the procedure proposed by Hoffmann and Schatz[1] for constructing Hamiltonian matrix elements. Because the spin−orbit Hamiltonian is totally symmetric, the seven states in our electronic basis (six triplets and one singlet) are parity decoupled as determined by their spin and spatial symmetry (here neglecting Coriolis interactions between electronic and nuclear orbital degrees of freedom), leading to two groups of coupled states. The group with four states includes the singlet state and three triplets, but the other includes only triplets. Because we are interested in ISC effects, only the four-state basis is considered for the detailed calculations. Because two of these four electronic basis functions are components of a common spin multiplet, we can consider only three Born−Oppenheimer surfaces for this four-state basis. The spin−orbit matrix elements that couple the Born−Oppenheimer states are determined using complete active space self-consistent field (CASSCF) methods because electron correlation is relatively unimportant for spin−orbit coupling.

As shown in Figure 1, the most important singlet−triplet crossings in the S + H_2 reaction are between the two lowest components of S(^{3}P), which have ^{3}A′ and ^{3}A″ symmetry for nonlinear SHH geometries, and the lowest component of S(^{1}D), which has ^{1}A′ symmetry for nonlinear SHH. In the absence of spin−orbit coupling, these states all correlate to the product ground state of SH($^2\Pi$). The results derived from full dimensional potential energy surfaces and CASSCF spin−orbit couplings give rise to asymptotic fine-structure splittings that are $E(^3P_1 \rightarrow {}^3P_2) = 184$ cm^{-1} and $E(^3P_0 \rightarrow {}^3P_1) = 180$ cm^{-1}. The corresponding experimental values are 398 and 174 cm^{-1}, respectively. We should add here that spin−orbit splittings for S(^3P) in the 15-state basis are $E(^3P_1 \rightarrow {}^3P_2) = 344$ cm^{-1} and $E(^3P_0 \rightarrow {}^3P_1) = 159$ cm^{-1}. A splitting of 325 cm^{-1} for SH($^2\Pi$) was found from our calculation.

Spin−orbit matrix elements were calculated using the Breit−Pauli method as implemented by Fedorov and Gordon[11] in GAMESS.[12] On the basis of the theory of Hoffmann and Schatz[1] noted above, we used the seven-state (^{3}A′, ^{3}A″, and ^{1}A′) basis in our calculation, and this was further decoupled into the following four states: ^{3}A′ ($M_s = 0$), ^{3}A″($M_s = \pm 1$), and ^{1}A′-($M_s = 0$). With these four states, there are five linearly independent nonzero off-diagonal spin−orbit matrix elements:

$$\langle {}^1A'(M_s = 0)|H^{SO}|{}^3A''(M_s = 1)\rangle$$

$$\langle {}^1A'(M_s = 0)|H^{SO}|{}^3A''(M_s = -1)\rangle$$

$$\langle {}^1A'(M_s = 0)|H^{SO}|{}^3A'(M_s = 0)\rangle$$

$$\langle {}^3A''(M_s = 1)|H^{SO}|{}^3A'(M_s = 0)\rangle$$

and

$$\langle {}^3A''(M_s = -1)|H^{SO}|{}^3A'(M_s = 0)\rangle$$

The matrix elements are complex numbers and are not used in our calculations directly. To get a real-valued Hamiltonian matrix, we combine the three components of the triplet wave function to form symmetry-adapted triplet wave functions that are purely imaginary-valued:

$$\begin{aligned} {}^3\Psi_z &= \mathrm{i}\,{}^3\Psi(M_s = 0) \\ {}^3\Psi_x &= \frac{\mathrm{i}}{\sqrt{2}}[{}^3\Psi(M_s = 1) - {}^3\Psi(M_s = -1)] \\ {}^3\Psi_y &= \frac{\mathrm{i}}{\sqrt{2}}[{}^3\Psi(M_s = 1) + {}^3\Psi(M_s = -1)] \end{aligned} \qquad (1)$$

To calculate the spin−orbit matrix elements, we have adopted a body-fixed Jacobi coordinate system with the z axis perpendicular to the plane and the positive x axis is defined as the vector from the center of mass of H−H to a particular H. These spin−orbit matrix elements then were fit using a bicubic spline function as a function of the Jacobi coordinates to obtain global spin−orbit matrix elements. The resulting spin−orbit matrix elements are plotted in Figure 4 in Jacobi coordinates (R, θ) at a fixed value of $r = 1.4a_0$. This Figure indicates how spin−orbit coupling matrix elements change when S approaches H_2 at its equilibrium geometry. It is worth pointing out here that the magnitudes of the spin−orbit matrix elements for SH_2 are about 3 times larger than for the OH_2 system, with values that vary between −240 and 240 cm^{-1}. To show the dependence of the spin−orbit coupling elements on the Jacobi coordinate r, we have plotted the same spin−orbit matrix elements in Figure 5 but at a fixed Jacobi angle $\theta = 60°$. This Figure indicates that spin−orbit matrix elements strongly depend on the diatomic distance.

B. Dynamics. We have used the quasiclassical variant of Tully's fewest-switches trajectory surface-hopping (TSH) method to study the S(^{3}P, ^{1}D) + H_2 reaction using the four electronic states described earlier. Our studies show that the minimum-energy crossing in the singlet−triplet intersection is below the triplet barrier; moreover, it is also below the product asymptote. This indicates that the SH + H products could predominantly form via the singlet potential energy surface. Quasiclassical binning was accomplished by representing the diatomic molecules by Morse oscillators using parameters given above. Diatomic reactants were prepared in ground rovibrational states.

On the basis of the theory proposed by Herman[13] and its application to our previous calculations,[2] we have adapted a "mixed" representation (smoothly switching between adiabatic and diabatic) of the space spanned by the four basis functions in the present calculation. We also report single surface calculations, for comparison, which elucidate the importance of ISC effects in the reaction dynamics. The reason for using the mixed representation, as examined in detail in our previous publication,[2] is that in the more conventional adiabatic representation there is unphysical behavior of the electronic populations due to a lack of coherence in the state evolution with the TSH method when the three closely spaced triplet states cross the singlet state. Because coherence is not maintained in the TSH algorithm and a statistical algorithm is used to determine hopping probabilities, there is a serious error in the TSH algorithm in describing the sharply avoided intersystem crossing using the adiabatic representation, and the adiabatic TSH probabilities overestimate the hopping probability for transition between the singlet and triplet manifolds. Instead, more accurate results are expected using a diabatic representation close to the singlet−triplet crossing because the hopping probabilities are

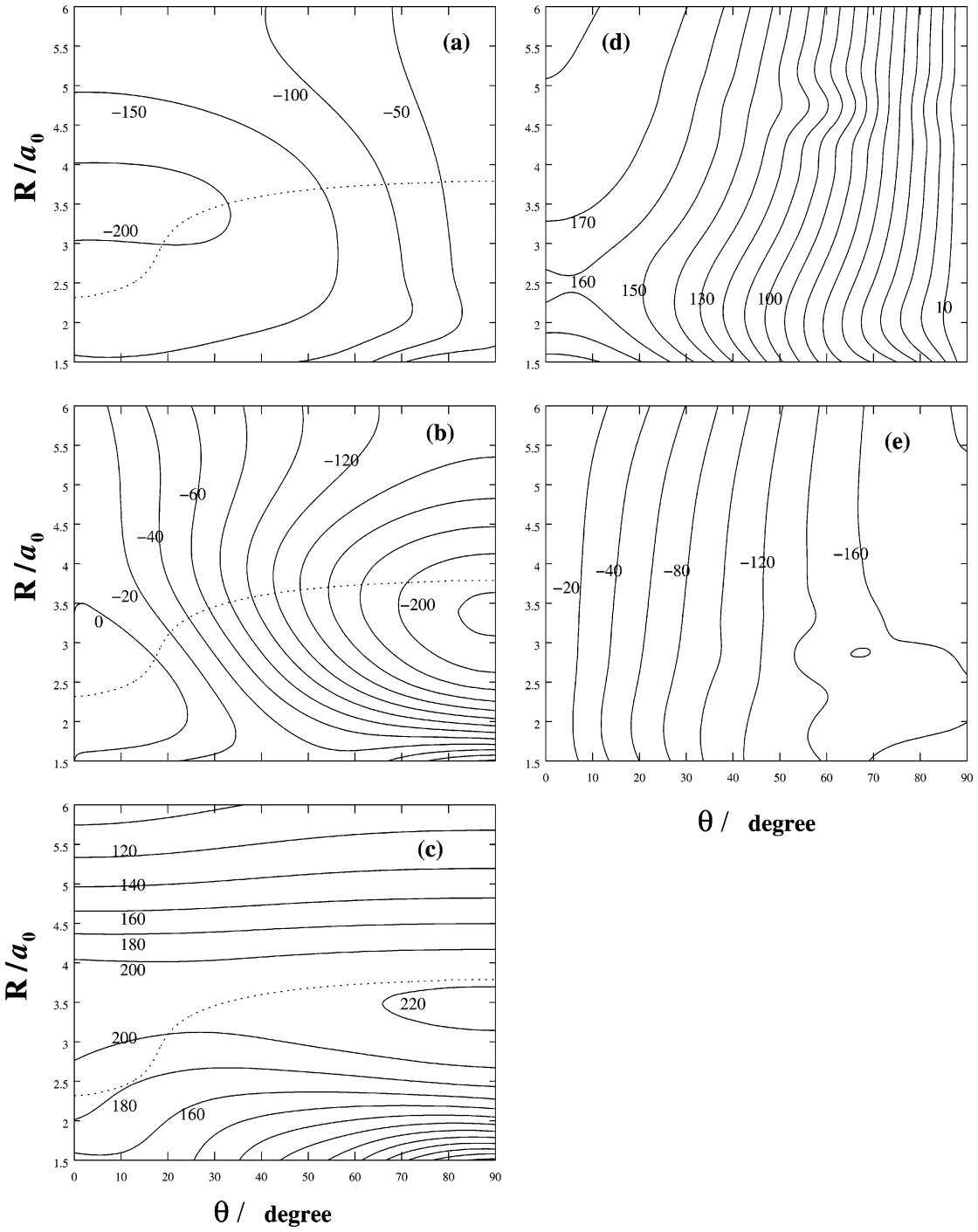

Figure 4. Contours of the spin−orbit matrix elements (in cm^{-1}) at $r = 1.40a_0$: (a) $\langle {}^1A'|H^{SO}|{}^3A_x''\rangle$; (b) $\langle {}^1A'|H^{SO}|{}^3A_y''\rangle$; (c) $\langle {}^1A'|H^{SO}|{}^3A'(M_s = 0)\rangle$; (d) $\langle {}^3A_x''|H^{SO}|{}^3A'(M_s = 0)\rangle$; (e) $\langle {}^3A_y''|H^{SO}|{}^3A'(M_s = 0)\rangle$.

small. However, the diabatic representation cannot describe the proper asymptotic states, which are defined only in the adiabatic representation. The mixed representation thus circumvents these problems as excess hopping in the intersection seam region is eliminated through the use of a diabatic treatment (in which the hopping probability is low because there is no derivative coupling and relatively weak spin−orbit coupling), whereas away from the reactive regions (i.e., reagent and product regions), an adiabatic representation is used (i.e., only derivative coupling is present, and spin−orbit interaction is included in the adiabatic surfaces). Between these two limits, the switching between adiabatic and diabatic representations is done smoothly.

The mixed representation is defined by writing the full (i.e., nonrelativistic plus spin−orbit) Hamiltonian in our four-state basis as a sum of diagonal and off-diagonal parts as follows:

$$H = H_{diag} + H_{off}$$

Here, H_{diag} and H_{off} are the diagonal and off-diagonal parts in a diabatic representation that is defined by the nonrelativistic eigenstates. Thus, the diagonal part of H contains the nonrelativistic potential surfaces, and the off-diagonal parts contain the spin−orbit coupling. The Hamiltonian H is now repartitioned to define a mixed representation (using $H = H_{mix} + H_{coup}$) in which one part, termed H_{mix}, defines the part of the Hamiltonian to be treated in the adiabatic representation and the remainder, H_{coup}, provides the potential coupling for the adiabats. To do this, we have defined H_{mix} and H_{coup} in terms of H_{diag} and H_{off}

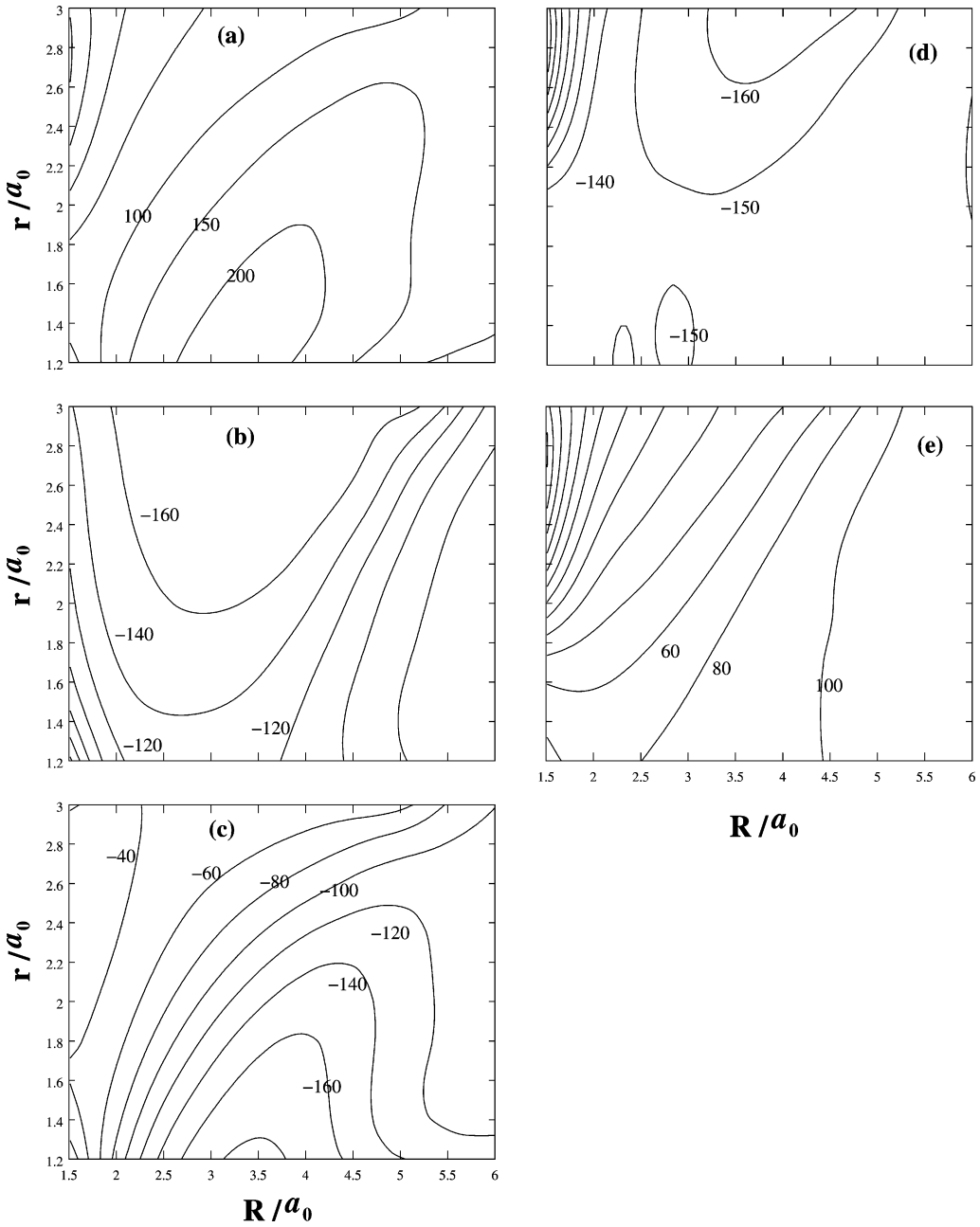

Figure 5. Same as for Figure 4 except at $\theta = 60°$.

via

$$H_{\text{mix}} = H_{\text{diag}} + \cos^2\phi\, H_{\text{off}}$$

$$H_{\text{coup}} = \sin^2\phi\, H_{\text{off}}$$

where ϕ is a switching angle that is chosen to be $\pi/2$ close to the crossing (where we have $H_{\text{mix}} = H_{\text{diag}}$ and the diabatic representation is recovered) and zero in the reagents and products (as $H_{\text{mix}} = H$ and the adiabatic representation is recovered). To complete the definition, we have chosen ϕ to be the product of three functions, two of which have the form $f(x) = [\tanh(\gamma(x - x_0)) - \tanh(\gamma'(x' - x'_0))]/2$. Here x denotes R or r, the reactant Jacobi coordinates, and x' denotes the corresponding product Jacobi coordinates. The third function is for the Jacobi angle θ and is defined as $f(\theta) = [1.0 + \tanh(\gamma(\theta - \theta_0))]/2$. x_0 and x'_0 are determined by the location of the singlet−triplet crossing seams, and overall we have $\phi = (\pi/2) f(R)\, f(r)\, f(\theta)$. The parameters used for the switching angle are listed in Table 2.

The system of partial integrodifferential equations for the electronic basis function coefficients $\hat{c}_k(t)$ in the mixed representation can be written as[2]

$$\begin{aligned}\text{Re}\dot{\hat{c}}_k = \frac{1}{\hbar}\sum_{j(\neq k)} \{H_{kj}[\cos\epsilon_{kj}\,\text{Im}\hat{c}_j - \sin\epsilon_{kj}\,\text{Re}\hat{c}_j] + \\ G_{kj}[\cos\epsilon_{kj}\,\text{Re}\hat{c}_j + \sin\epsilon_{kj}\,\text{Im}\hat{c}_j]\}\end{aligned}$$

$$\begin{aligned}\text{Im}\dot{\hat{c}}_k = \frac{1}{\hbar}\sum_{j(\neq k)} \{H_{kj}[-\cos\epsilon_{kj}\,\text{Re}\hat{c}_j - \sin\epsilon_{kj}\,\text{Im}\hat{c}_j] + \\ G_{kj}[\cos\epsilon_{kj}\,\text{Im}\hat{c}_j - \sin\epsilon_{kj}\,\text{Re}\hat{c}_j]\}\end{aligned} \quad (2)$$

Here $\hat{c}_j$ is the interaction picture coefficient of the jth basis function, and H_{kj} is the diabatic coupling matrix element associated with the off-diagonal Hamiltonian H_{coup} given above. Also, **G** is defined as $\mathbf{G} = (d\tilde{\mathbf{U}}/dt)\mathbf{U}$, with **U** being the

TABLE 2: Parameters for Switching Angle ϕ

parameters	values
$(R_0, R_0')/a_0$	(2.0, 5.0)
(γ_R, γ_R')	(3.0, 3.0)
$(r_0, r_0')a_0$	(0.7, 2.5)
(γ_r, γ_r')	(3.0, 3.0)
θ_0/deg	30.0
γ_θ	2.0

transformation matrix from the diabatic to the mixed representation eigenfunctions (i.e., the eigenvector matrix associated with H_{mix}) and $\tilde{\mathbf{U}}$ being the transpose of $\mathbf{U}$. $\epsilon_{kj}(t)$ in the above equations describes the time dependence of the integrals of the difference potentials:

$$\epsilon_{kj}(t) = \int_0^t \frac{E_j(t') - E_k(t')}{\hbar}\,\mathrm{d}t' \qquad (3)$$

where $E_j (j = 1-4)$ are the mixed representation eigenvalues. (One should note that here we refer to the eigenfunctions of H_{mix} as states that are "adiabatic in the mixed representation".) Although there is both potential coupling and derivative coupling in the mixed representation, the additional computational effort to treat both of these is very marginal when compared to the strict diabatic or strict adiabatic calculations.

To solve these equations as well as Hamilton's equations of motion for trajectory motion, we used a fifth-order predictor, sixth-order corrector algorithm with a maximum time step of 1.0 au. A smaller (0.5-au) time step reproduces the results within the statistical uncertainty of our calculations (3% for the larger cross sections). Trajectories (30 000) were evaluated for each energy, and the maximum impact parameter used was $10a_0$.

As discussed in our earlier publication,[2] the implementation of the TSH algorithm in the mixed representation is subtly different from the usual TSH algorithm.[14] The adiabats do not cross, and the states can be connected from one time step to the next by simply ordering them by energy. Unless there is a hop, the current energy-ordered state used to determine forces for the trajectory propagation does not change. However, near the crossing seam when the dynamics is completely diabatic the connection between states along a trajectory is determined by the maximum overlap of the states from one step to the next. Therefore, in the mixed representation we need to switch from the adiabatic connection procedure to the diabatic connection procedure based on the value of the switching angle ϕ. In the present calculations, the value of the angle ϕ was monitored during the trajectory propagation, and when it drops below a cutoff value 0.14 rad, the state assignment is switched from adiabatic to diabatic. The assignment algorithm is reversed when the value rises above 0.14 rad. We have examined results for other values of this cutoff and have found that the results are not sensitive if we reduce this value further.

III. Results and Discussion

A. Potentials and Couplings. In the truncated spin-adapted basis described above, there are three potential energy surfaces required in our calculations for the S + H_2 reaction, corresponding to $^3A'$, $^3A''$, and $^1A'$ for nonlinear geometries of S−H−H. In the singlet PES, reaction proceeds through the formation of an intermediate complex SH_2, which as noted in Figure 1 corresponds to a potential well of −94.4 kcal/mol with respect to the product asymptote. This is based on the surface of Ho et al.[10] and is very close to the experimental value (after removing the zero-point contribution) that we estimate to be −95.0 kcal/mol.[7] However, in the triplet surfaces there is a barrier to reaction of about 25.3 kcal/mol based on the QCISD(T) calculations. In the reagent asymptote, the singlet state is 27.7 kcal/mol above the triplet states in the absence of spin−orbit coupling. (The experimental value is 26.4 kcal/mol.[7]) In the product region, the singlet and triplet states are degenerate if spin−orbit couplings are not considered. In the presence of SO coupling, the reagent fine structure triplet-state energies are −24.0 ($^3P_2$), −23.5 ($^3P_1$), and −23.0 kcal/mol ($^3P_0$), and product fine structure energies are −0.5 ($^2\Pi_{3/2}$) and 0.5 kcal/mol ($^2\Pi_{1/2}$). The zero-point energy difference between the reagents and products is 2.4 kcal/mol. Therefore, the effective reactive thresholds for the three reagent fine structure triplet states are 21.2, 20.7, and 20.2 kcal/mol for $^3P_2$, $^3P_1$, and $^3P_0$, respectively. The experimental reaction endothermicity (at 0 K) is 19.8 kcal/mol,[7] so the calculated $^3P_2$ result is 1.4 kcal/mol too high.

Figures 2 and 3 show contours of these potential energy surfaces along with the intersection seam (plotted with a dashed line) to illustrate the portions of the PESs that are relevant to intersystem crossing effects. It is discernible from these Figures that the minimum along the singlet−triplet crossing seam is below the triplet barrier and, moreover, below the product asymptote. This clearly suggests that unlike the O + H_2 reaction S + H_2 can follow a spin-forbidden pathway from the reactants to the products, which could be the predominant reaction mechanism.

The variation of the spin−orbit matrix elements as a function of Jacobi coordinates (R, θ) at a fixed $r = 1.4a_0$ is presented in Figure 4 using our spin-adapted four-state basis. This tells us how the spin−orbit matrix elements evolve as the S atom approaches H_2. Dotted lines show the location of the singlet−triplet crossing seam, which is where the coupling elements play an important role in the ISC process. It is worth pointing out here that in addition to the crossing-seam region spin−orbit coupling is important in the reagent and product regions even though no crossings occur. For large R, we see that asymptotic behavior is apparent only for R larger than $5.0a_0$. This is to be compared with the asymptotic behavior of the potential surfaces, which is also close to being converged at $5.0a_0$. Although there are not many oscillations in the spin−orbit matrix elements for the SH_2 system when compared with OH_2 (cf. Figure 4 with Figure 4 of Maiti and Schatz[2]), the shapes of the spin−orbit surfaces for OH_2 and SH_2 are similar. However, the SH_2 amplitudes are about 3 to 4 times larger. We also found that the minimum energy on the crossing seam corresponds to the T-shaped geometry of SH_2; it is therefore expected that the matrix element $\langle {}^1\Psi' | H_{\mathrm{SO}} | {}^3\Psi_x'' \rangle$ shown in Figure 4a plays no significant role in ISC because the magnitude of the spin−orbit coupling is very small for perpendicular structures. In addition, even though the matrix elements $\langle {}^3\Psi' | H_{\mathrm{SO}} | {}^3\Psi_y'' \rangle$ and $\langle {}^3\Psi' | H_{\mathrm{SO}} | {}^3\Psi_y'' \rangle$ are not directly connected to the singlet−triplet crossing, they have a significant effect on ISC processes as they are important to the asymptotic splittings.

The spin−orbit matrix elements are strongly dependent on the Jacobi coordinate r. This is demonstrated in Figure 5, where we have plotted the same matrix elements as in Figure 4 but versus r and R for $\theta = 60°$. This indicates that one needs to include the dependence on r in the TSH calculation.

B. TSH Results. We have carried out TSH calculations to study the S + H_2 reaction dynamics for an energy range from 20 (close to the reactive threshold) to 50 kcal/mol. An inspection of several individual trajectories showed that a large number of reactive trajectories starting in the triplet surfaces cross to the singlet during reaction and spend a significant amount of time in the singlet well before going to products. In Figure 6,

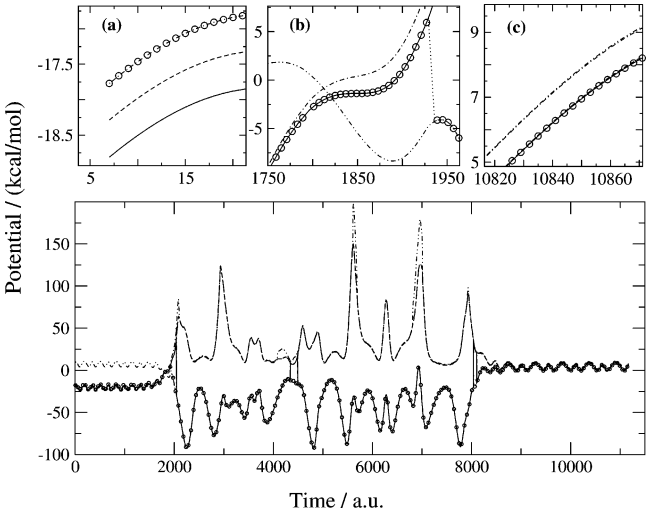

Figure 6. Singlet ($^1A'$) and triplet ($^3A'$, $^3A''$) potentials as a function of time for geometries along a particular reactive trajectory. The surface that governs the trajectory motion is indicated by open circles connected by a dotted line. Top panel: (a) starting point of the trajectory in the $^3P_0$ state; (b) singlet−triplet crossings along with the reactive trajectory hopping from one of the triplet surfaces to the singlet state $^1A'$, and (c) two doubly degenerate product states, with the trajectory ending up in $SH(^2\Pi_{3/2})$.

we have plotted potentials as a function of time for one such trajectory that has an energy of 36 kcal/mol. The line with the open circles connected by dotted lines refers to the potential surface that the trajectory is "on" at each point, implying that this surface is used to define the forces to solve the equations of motion, providing the reference point for calculating the hopping probability. In the top panel in Figure 6, there are three plots. Figure 6a represents the first femtosecond of the trajectory starting in the $^3P_0$ state. Figure 6b depicts the singlet−triplet crossing region in which the reactive trajectory hops from one of the triplet surfaces to the singlet state $^1A'$. This also emphasizes that the minimum-energy crossing is below the product asymptote (taken to be the zero of energy). Figure 6c shows the two doubly degenerate product states $SH(^2\Pi_{3/2}$ and $^2\Pi_{1/2}) + H$, with the trajectory ending up in $SH(^2\Pi_{3/2})$. The bottom panel shows that the trajectory spends most of its time in the singlet well.

Because our calculation is based on a four-state Hamiltonian in the mixed representation, where both of the asymptotes are treated adiabatically, we are able to determine fine-structure-resolved cross sections for both reagents and products. More precisely, we are able to predict the spin−orbit distribution for the product states $SH(^2\Pi_{3/2}) + H(^2S_{1/2})$ and $SH(^2\Pi_{1/2}) + H(^2S_{1/2})$ starting from each of the fine-structure states $^3P_2$, $^3P_1$, and $^3P_0$ of the reactants.

Integral cross sections for the reaction $S + H_2$ are presented in Figures 7−10. Figure 7 shows results for the $^3P_2$ initial state, including branching to the two spin states $^2\Pi_{3/2}$ and $^2\Pi_{1/2}$ of the product SH. In this case, the cross section for reaction to the lower spin state $^2\Pi_{3/2}$ is about a 4 times larger than that to the higher spin state $^2\Pi_{1/2}$. In other words, reaction starting in the lowest reagent spin state $^3P_2$ leads predominantly to the adiabatic product. When trajectories start in $^3P_1$ (as shown in Figure 8), there is more significant nonadiabatic dynamics, with the lower-state cross section (the adiabatic product) being comparable to the upper-state cross section for energies <36 kcal/mol. Figure 9 shows that the two possible product states have about the same cross sections for the $^3P_0$ initial state, for energies below 26 kcal/mol (note that the barrier is 25.3 kcal/mol), and then the higher spin state (the adiabatic state) is predominant at higher energies. Overall, these results indicate that the $S + H_2$ dynamics is significantly more nonadiabatic than the $O + H_2$ dynamics.

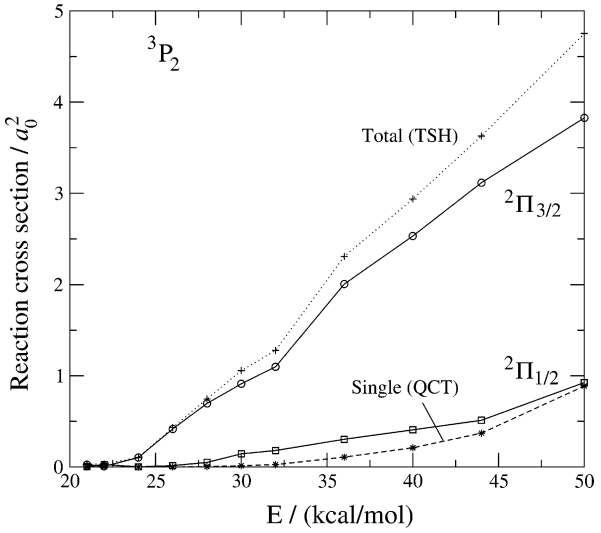

Figure 7. Integral cross sections as a function of collision energy for $S(^3P_2) + H_2$. Solid curves represent cross sections for the full Hamiltonian to specific product states, dotted curves (with +) show the sum over product states, and dashed curves (with *) show the single-surface calculations, where couplings are not taken into account. Circles indicate trajectories associated with the $SH(^2\Pi_{3/2}) + H$ state, and squares refer to $SH(^2\Pi_{1/2}) + H$. The single-surface calculations refer to the $^3A''$ potential surface.

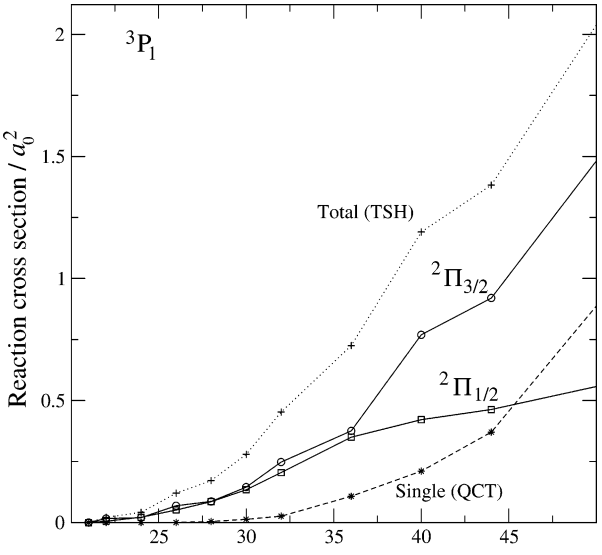

Figure 8. Same as for Figure 7 except for $S(^3P_1) + H_2$. The single-surface calculations refer to the $^3A''$ surface.

For the triplet initial state, we see in Figures 7−9 that there is a significant reaction probability for collision energies that are below the barrier to reaction (25.3 kcal/mol). Although it was inferred from experimental data that the activation energy is comparable to the reaction endothermicity,[7] it was also argued that the preexponential factor was too large to be appropriate for a spin-forbidden reaction. To explore this issue we have performed single-surface calculations for the triplet states, and the resulting reaction cross sections are included in Figures 7−9 for comparison. It is obvious from these Figures that the single-surface reaction cross sections (labeled QCT) are significantly smaller in magnitude than the coupled surface results for all

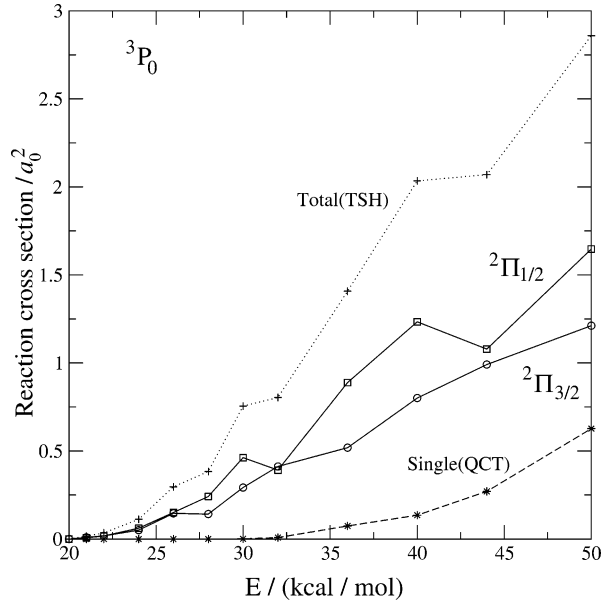

Figure 9. Same as for Figure 7 except for $S(^3P_0) + H_2$. The single-surface calculations refer to the $^3A'$ surface.

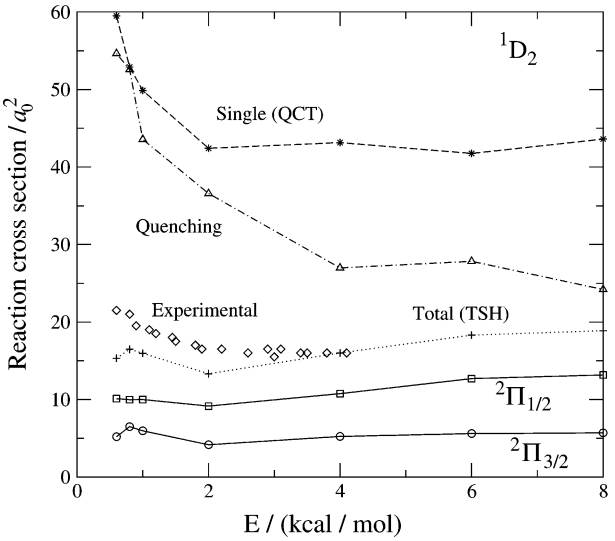

Figure 10. Same as for Figure 7 except for $S(^1D_2) + H_2$. The single-surface calculations refer to the $^1A'$ surface. Also included is the TSH quenching cross section and experimental data for the reactive cross section taken from Liu and co-workers[15] and normalized to the calculated value at 4 kcal/mol.

energies under investigation. This difference is large near the reactive threshold and decreases slowly with increasing energy. The single-surface results show that the reaction threshold is at about 29 kcal/mol for both the $^3A''$ and $^3A'$ surfaces. This is in accord with the zero-point-energy-corrected saddle-point energy with respect to reagents. This shows that the excess reactivity at low energies (below the threshold) is solely due to intersystem crossing.

In Figure 10, we present the reaction cross section as a function of collision energy for trajectories starting in the singlet state $^1D_2$. There is no barrier to reaction on the singlet surface and the reaction is exothermic, so the cross section decreases with energy. However, note also that the single-surface reaction cross section is much larger than the coupled-surface cross section, even after summing over final states. This occurs because there is strong electronic-state quenching leading to $S(^3P) + H_2$. The quenching cross section is plotted in the Figure,

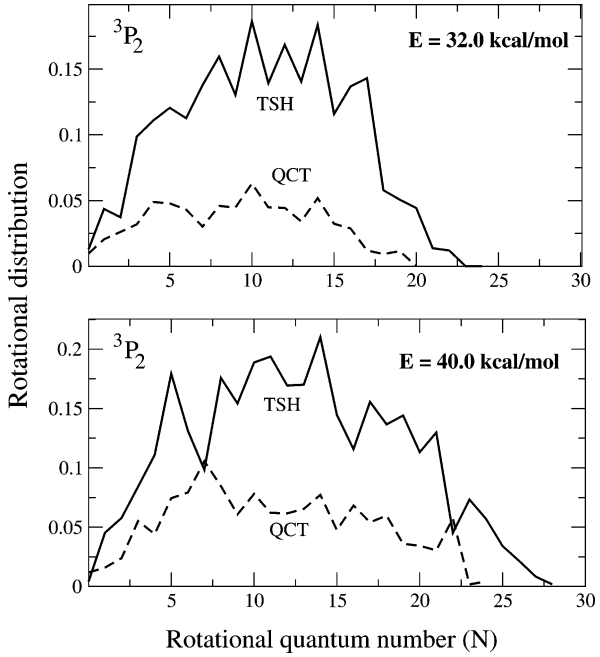

Figure 11. Product rotational distributions for the initial state $^3P_2$. TSH results (solid line) are compared with the corresponding single-surface results (dashed line).

and we see that it is larger than the reactive cross section at low energy. Indeed, trajectories that undergo intersystem crossing (singlet-to-triplet transition) are more likely to go to $S(^3P) + H_2$ than to SH + H because the singlet−triplet crossing is before the triplet barrier.

Also plotted in Figure 10 is an experimental estimate of the reactive cross section from Lee and Liu.[15] This measurement determines only the relative cross section, so we have normalized it to our result at 4 kcal/mol. We see that the measured cross section shows the relatively weak energy dependence in the cross section that we find. Previously,[10] the measured cross section was compared to single-surface calculations, and it was found that the single-surface cross section has a stronger dependence on energy, dropping more rapidly with increasing collision energy than is seen in the measurements (as can be seen in Figure 10). This was in contrast to analogous comparisons of cross sections for the $O(^1D) + H_2$ reaction, where the measured excitation function was in good agreement with single-surface calculations at low energy.[3] Previously, we found that quenching is not very important to $O(^1D) + H_2$,[2] so the single-surface result is a good approximation (at least at low energy where excited singlet states do not contribute). However, here we see that quenching is quite important for $S(^1D) + H_2$, and this is why single-surface results and experiment are not in good agreement. Of course, the role of excited singlet states in $S(^1D) + H_2$ is also a point of uncertainty, but we expect that these will become important only at energies above 5 kcal/mol.

Product rotational distributions for the $S + H_2$ reaction at 32.0 and 40.0 kcal/mol are presented in Figures 11 and 12 for the initial states $^3P_2$ and $^3P_0$, respectively. Included are results from single-surface calculations for comparison. For both initial states and at both energies, we see excess product SH rotational excitation from the TSH calculations. This results from trajectories that hop to the singlet state and experience the deep singlet well leading to higher rotational excitation than on the triplet surfaces. As with the $O + H_2$ reaction, the effect is more noticeable at lower translational energy, where product rotational excitation, comparatively, is smaller.

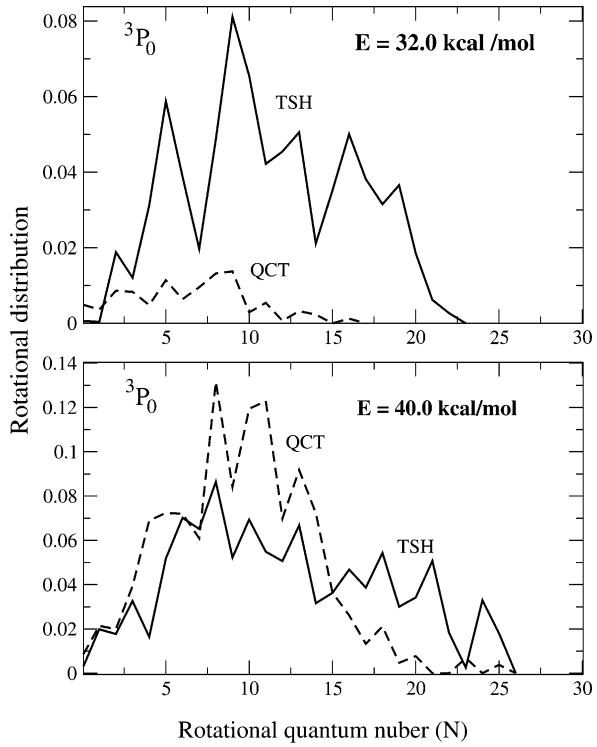

Figure 12. Results analogous to those shown in Figure 11 but for the initial state $^3P_0$.

The rate constant for the $S(^3P) + H_2$ reaction is too small to be measured experimentally at room temperature. However, at higher temperature, (e.g., $T = 1000$ K), the measured rate constant is $\sim 9.53 \times 10^{-15}$ cm^3 molecule^{-1} s^{-1}.[7] Using the results in Figures 7−9, one can estimate a thermal rate constant of 0.44×10^{-16} cm^3 molecule^{-1} s^{-1} for the ground rotational state. This result assumes that the reactive threshold energy for the $^3P_2$ state of S is the value for the potential surfaces we used, 21.2 kcal/mol. As mentioned earlier, the correct threshold energy is 19.8 kcal/mol, so if the threshold is lowered to this value, the rate constant is increased by a factor of 2.0 to 0.88×10^{-16} cm^3 molecule^{-1} s^{-1}. This is well below the experimental value, which suggests that rotationally excited states must have a much larger rate constant than the ground state. Indeed, because complex formation can occur at energies below the product asymptote, one might imagine that reagent rotational excitation will serve to lower the reactive threshold by an amount equal to the reagent rotational energy. If we make this assumption and evaluate the rate constants using the $j = 0$ cross sections as above and further include the factor of 2.0 correction just described, we obtain a rate constant of 11.4×10^{-15} cm^3 molecule^{-1} s^{-1}, which is in the range of experimental results noted by Shiina et al. To test this model, we have used the TSH method to calculate cross sections for selected rotational states. We find that the threshold is indeed lowered by rotational excitation, however not by as much as in the simple model. When we fit these cross sections and again include the factor of 2.0 correction, our best estimate of the rate constant is 2.6×10^{-15} cm^3 molecule^{-1} s^{-1}. The fact that this is well above the $j = 0$ result but below the experimental value shows the extreme sensitivity of the results to details of coupled surface dynamics near the point of crossing of the singlet and triplet states and suggests that further refinement of the surfaces (and perhaps dynamics) is needed to model the experiments successfully. An additional question is, how important are quantum effects in the reaction dynamics? Unfortunately, developing the quantum methods in three dimensions for four coupled states is a difficult task.

IV. Summary and Conclusions

We have studied intersystem crossing effects in the $S + H_2$ reaction by performing TSH calculations using a mixed representation approach in a truncated and decoupled four-state basis. Coriolis interactions between the spatial and spin coordinates were neglected, but spin−orbit coupling elements were determined in full dimensionality to describe the intersystem coupling among the states.

TSH calculations based on the mixed representation show that the spin−orbit interactions lead to a dramatic change in the reaction cross sections for the $S(^3P) + H_2$ reaction, especially near the threshold. This arises because spin−orbit-induced intersystem crossing permits the reaction to occur without surmounting the triplet barrier. In addition, we see excess product rotational excitation resulting from trajectories that sample the deep singlet well before forming products.

Although intersystem crossing is not very important to the $O + H_2$ reaction, for $S + H_2$ we find that the reaction rate at room temperature is predominantly determined by intersystem crossing effects. Whereas in the $O + H_2$ reaction the fine-structure-resolved dynamics is mostly adiabatic, we find in the $S + H_2$ reaction that there are significant nonadiabatic transitions leading to product fine structure distributions that have considerable populations in both states of SH.

Finally, we discovered that spin−orbit interactions have an important effect on the $S(^1D) + H_2$ reaction, leading to a quenching cross section that at low energy is larger than the reactive cross section. This gives the reactive cross section a weaker dependence on collision energy than is seen in the single surface dynamics, which is a result that agrees quantitatively with recent molecular beam measurements.

Acknowledgment. This work has been supported by NSF Grant CHE-0131998 (G.C.S.), by the Hungarian National Research Fund Grant OTKA T34812 (G.L.), and by a NSF-Hungarian Scientific Research Fund-Hungarian Academy of Sciences collaboration (grant no. 006). We thank Diego Troya and Mark R. Hoffmann for helpful discussions and Rex Skodje for a copy of the singlet potential surface.

References and Notes

(1) Hoffmann, M. R.; Schatz, G. C. *J. Chem. Phys.* **2000**, *113*, 9456.
(2) Maiti, B.; Schatz, G. C. *J. Chem. Phys.* **2003**, *119*, 12360.
(3) Garton, D. J.; Minton, T. K.; Maiti, B.; Troya, D.; Schatz, G. C. *J. Chem. Phys.* **2003**, *118*, 1585.
(4) Shiina, H.; Oya, M.; Yamashita, K.; Miyoshi, A.; Matsui, H. *J. Phys. Chem.* **1996**, *100*, 2136.
(5) Woiki, D.; Roth, P. *J. Phys. Chem.* **1994**, *98*, 12958.
(6) Olschewski, H. A.; Troe, J.; Wagner, H. Gg. *J. Phys. Chem.* **1994**, *98*, 12964.
(7) Shiina, H.; Miyoshi, A.; Matsui, H. *J. Phys. Chem. A* **1998**, *102*, 3556.
(8) Binoist, M.; Labégorre, B.; Monnet, F.; Clark, P. D.; Dowling, N. I.; Huang, M.; Archambault, D.; Plasari, E.; Marquarie, P.-M. *Ind. Eng. Chem. Res.* **2003**, *42*, 3943.
(9) Tsuchiya, K.; Yamashita, K.; Miyoshi, A.; Matsui, H. *J. Phys. Chem.* **1996**, *100*, 17202.
(10) Ho, T.-S.; Hollebeek, T.; Rabitz, H.; Chao, S. D.; Skodje, R. T.; Zyubin, A. S.; Mebel, A. M. *J. Chem. Phys.* **2002**, *116*, 4124.
(11) Fedorov, D. G.; Gordon, M. S. *J. Chem. Phys.* **2000**, *112* 5611.
(12) Schmidt, M. W.; Baldridge, K. K.; Boatz, J. A.; Elbert, S. T.; Gordon, M. S.; Jensen, J. H.; Koseki, S.; Matsunaga, N.; Nguyen, K. A.; Su, S. J.; Windus, T. L.; Dupuis, M.; Montgomery, J. A. *J. Comput. Chem.* **1993**, *14*, 1347.
(13) Herman, M. F. *J. Chem. Phys.* **1999**, *111*, 10427.
(14) Schatz, G. C.; Pederson, L. A.; Kuntz, P. J. *Faraday Discuss.* **1997**, *108*, 357.
(15) Lee, S.-H.; Liu, K. *Chem. Phys. Lett.* **1998**, *290*, 323.